

## Large flares (M1 – X7) in solar cycle 24

E.A. Bruevich <sup>a</sup>, T.V. Kazachevskaya <sup>b</sup>, G.V. Yakunina <sup>a</sup>

<sup>a</sup> *Sternberg Astronomical Institute, Lomonosov Moscow State University,  
Universitetsky pr., 13, Moscow 119234, Russia*

<sup>b</sup> *Fedorov Institute of Applied Geophysics  
Rostokinskaya, 9, Moscow, 129128, Russia*

*e-mail: red-field@yandex.ru, kazachevskaya@mail.ru, yakunina@sai.msu.ru*

### ABSTRACT

The large (X-ray class  $> M1$ ) and very large (X-ray class  $> X1$ ) flares (according to the observations of GOES-15 and Preliminary data from Current Catalog of Flare Events) in solar activity cycle 24 were analyzed. The monthly average values of optical Flare Index for 2010 – 2016 were calculated. The values of the total energy of the flare  $E$  ( $J \cdot m^{-2}$ ) in the 0.1 – 0.8 nm range at the level of the earth's atmosphere were estimated. The energy spectrum (the dependence of the number of flares with the full energy  $E$  from the value of this full energy) for 115 flares of M5 – X7 classes was built. The comparative study of monthly averaged values of several indices of solar activity in current cycle 24: the relative sunspot numbers (SSN), the 10.7 cm radio flux ( $F_{10.7}$ ), the radiation flux in the Lyman-alpha line ( $F_{L\alpha}$ ), the solar constant (TSI) and the Flare Index (FI) was made.

*Key words:* Solar activity, cycle 24, energy spectrum of large flares

## 1 Introduction

Cycle 24 has already proved to be quite different from recent cycles. Solar cycle 24 has started on December 2008, but according to the observations of global solar indices there was the minimal activity until early 2010. The previous sunspot archive data since accurate records began in 1850 show that solar cycle 24 is one of the lowest during the cycles with recorded sunspot activity. It was shown that there is the opposite long-scale trends during solar cycles 22 – 24, [Bruevich and Yakunina, 2015; Khlystov and Somov, 2012; Khlystov, 2014].

[Nagovitsyn et al., 2012; Pevtsov et al., 2014] have analyzed the recent SSN observations from [Pevtsov et al., 2011]. It was shown that in the recent times the number of large sunspots was decreased, but the number of small sunspots was increased. This change can be explained by the gradual decline in average sunspot field strength in accordance with the observation data. At the end of the XX-th and in the beginning of the XXI-st centuries we can see the minimum similar to the minimum of Dalton (the period of low SSN corresponding to low solar activity, lasting from about 1790 to 1830) and this current minimum is possibly a result of the superimpose of the 11-yr minimum on the minima of the 50-yr and the 100-yr cycles. SSN and  $F_{10.7}$  as the good indicators of solar activity show the reduction of their maximum values in cycle 24 equal to approximately 30 – 40%.

Flare activity in solar cycles 23 and 24 also differ significantly from previous cycles 21 and 22, this can be seen from Figure 1. Flares appear in areas with a complex structure of the magnetic field, which plays a determining role in flare's occurrence. During the powerful flares the fast processes cover huge areas which are continued from the photosphere to the corona. Flares reflect the energetics of magnetic fields and the behavior of parameters of flares in the 11-year cycle are of considerable interest. We used data from observations of  $F_{10.7}$ , SSN, and other solar indices from the archives of NOAA National Geophysical Data. Analysis in the EUV-region of the spectrum is the essential part of a studying of the processes of solar flares. The radiation in this spectral region (generated in the upper layers of the chromosphere and the transition layer) characterizes the conditions of these regions of the solar atmosphere during the development of flare. Observations in the EUV-region are significantly complementing our knowledge on the mechanisms of development of flares [Nusinov and Kazachevskaya, 2006].

Avakyan and Voronin, [2012] have analyzed the sun-weather-climate connections. They showed that there is a link between the processes occurring in the atmosphere of the earth and the level of solar-geomagnetic activity including solar flares. Thus, the task of studying of variations in solar activity is now becoming very relevant in connection with the problem of global warming in which the solar activity (in particular the flare activity) along with the human activity factor plays a significant role.

The aim of the work is the analyzing of the flare activity of the Sun in cycle 24 and the comparison of the fluxes during the evolution of the large flare of X6.9 class according to GOES-15 (Geostationary Operational Environmental Satellite) and SDO (Solar Dynamics Observatory) observations in the range

of wavelengths from the soft X-ray to the extreme ultraviolet.

## 2 FLARE ACTIVITY IN CYCLE 24

We have analyzed the data of the catalogue «Preliminary Current Catalog of Solar Flare Events with X-ray Classes M1 – X17.5 24-th cycle of Solar Activity (I.2009 – XII.2015)» available at [http://www.wdcb.ru/stp/data/Solar\\_Flare\\_Events/FI\\_XXIV.pdf](http://www.wdcb.ru/stp/data/Solar_Flare_Events/FI_XXIV.pdf). We have selected the 115 flares of M5 – X7 classes and 45 flares of X1 – X7 classes, which occurred on the Sun from February 2010 to December 2015. We have also calculated the solar Flare Index (FI) in accordance with the generally accepted standards from almost during the whole 24-th cycle is approximately proportional to the total energy emitted by a flare:  $FI = i \cdot t$ , where  $i$  is the intensity scale of importance defined in [Atac, 1987] and  $t$  is the duration of the flare in minutes. In Figure 1 the variations of the SSN, the  $F_{10.7}$  and the FI in the cycles 21 – 24 are shown. The general level of activity (according to observations of the SSN and the  $F_{10.7}$ ) in cycle 23 is slightly reduced, and in cycle 24 it decreases rather strongly (by about 30% in the maximum of cycle 24 compared to the previous maximums).

In [Bruevich et al., 2014] it was shown that the dependence of FI versus the overall level of solar activity in cycles 21 – 23 varies from cycle to cycle. Figure 1 shows that the FI is very much decreases in cycle 24, its value in the maximum of cycle 24 is almost 2 times less than in the maximums of cycles 21 and 22 [NOAA, 2016].

Atac [1987] noted that FI is one of the best indicators of activity variations in the chromosphere. It is of value as a measure of the short lived (minutes to hours) activity on the Sun. This feature makes the FI a suitable full disk solar index for comparison with similar solar indices which reflect different physical conditions from the different layers of the solar atmosphere.

Figure 2 shows the relationships between the FI versus the SSN, the solar constant TSI, the Mg II c/w (280 nm) index and the radiation flux  $F_{L\alpha}$ . Good correlation was found between FI and SSN, Mg II c/w index and the  $F_{L\alpha}$ , but not so good correlation exists between FI and TSI. The coefficients of linear correlation of FI versus other indices in cycle 24 are about 0.65 – 0.75. A closer correlation between FI and other solar indices were observed in cycles 21 – 23, the coefficients of linear correlation were about 0.75 – 0.85,

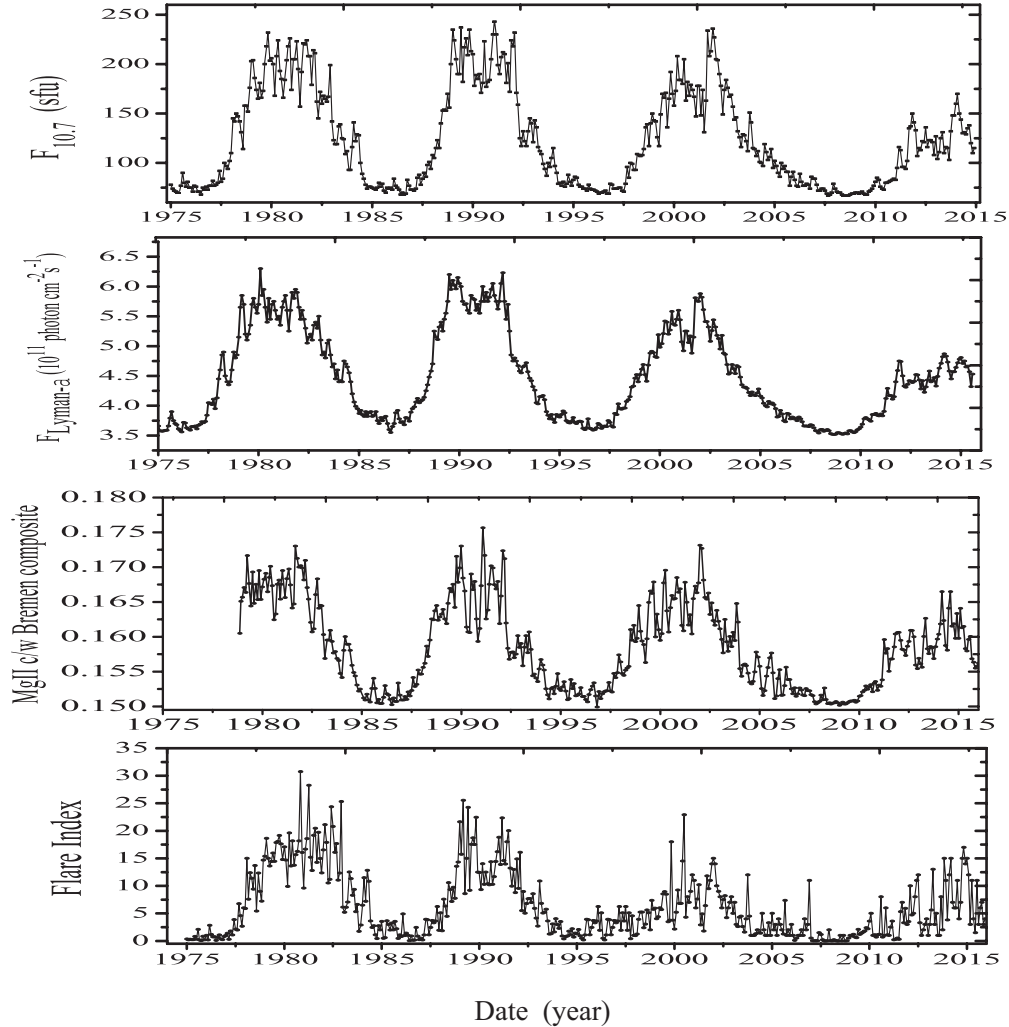


Figure 1: Time series of solar activity indices – monthly average values of SSN,  $F_{10.7}$  and Flare Index (FI).

[Bruevich et al. 2014].

Figure 3 shows the distribution of monthly average of number of flares M1 – X7 (more than 700 flares) in cycle 24. It is seen that the maximum number of flares (M1 – X7) does not coincide with the maxima of the number of spots in cycle 24, with the exception of 2014. We noted that the greatest number of flares in cycle 24 occurred in the decline phase after the first

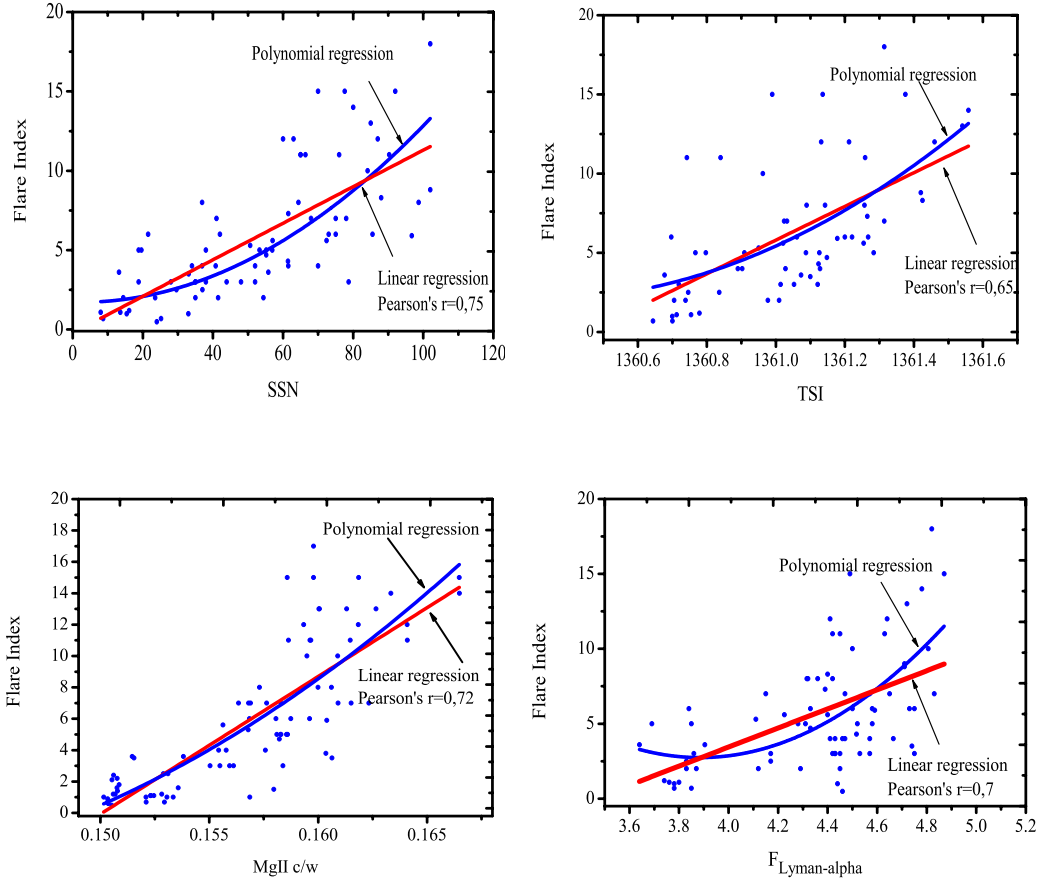


Figure 2: The relationship of monthly values of FI versus SSN, TSI, MgII c/w and  $F_{L\alpha}$  in cycle 24. The linear and polynomial regressions are shown.

maximum, during the second maximum and in the decline phase after the second maximum. The largest flares of cycle 24 of the X-ray class  $> X2.7$  occurred on rise phase and in the maximum. But in cycles 21 – 23 the largest flares of the X-ray class  $> X9$  were observed on the decline phases of cycles 21 and 23, as well as at the maximum of cycle 22, [Klystov, 2014].

The distribution of the number of flares (monthly average) in cycle 24 is shown in Figure 4. The strong flares (class  $> X2.8$ ) are pointed with the arrows. The months when numbers of flares (M1 – X7 classes) for a month

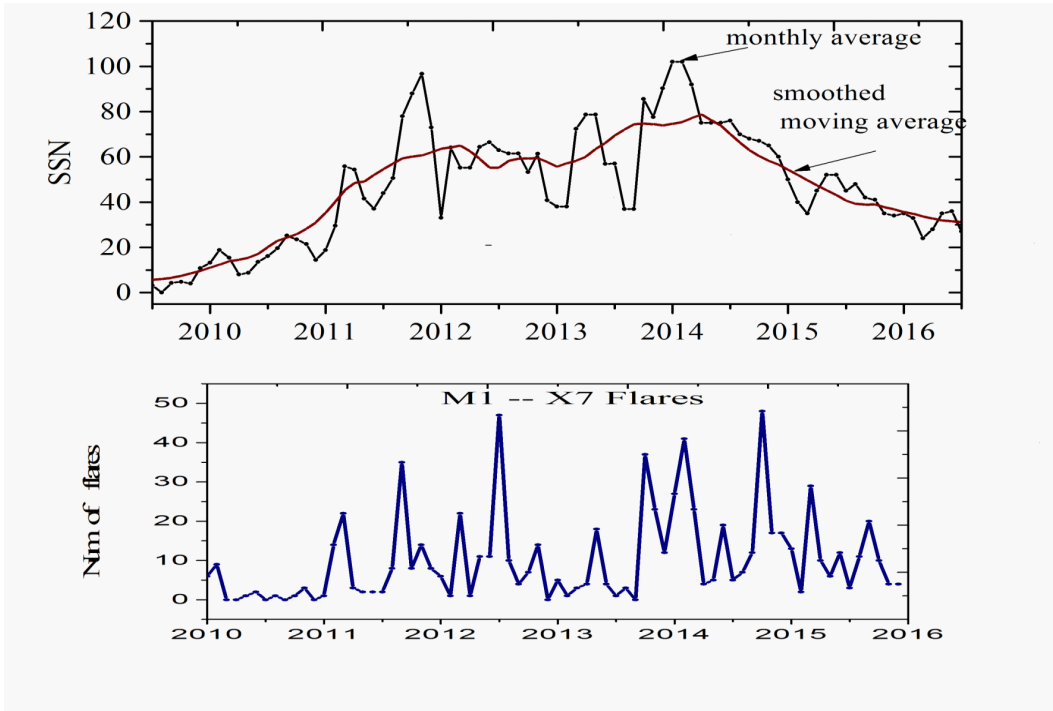


Figure 3: The distribution of monthly average of the number of flares of M1–X7 classes (about 700 flares) in cycle 24. The maximum of the number of flares (M1–X7 classes) do not coincide with the maximum of the number of spots in cycle 24, with the exception of 2014.

are less than 10 are pointed with the small circles. The months when numbers of flares are more than 10 flares per month are pointed with the big circles. Note then the greatest number of flares occurred after the first maximum, in the second maximum, and at the decline phase of cycle 24. The largest X-ray flares of classes X2.8 and more strong flares occurred during the rise phase and in the maximum phase of cycle 24.

There is very important to the study of such parameters of the flares. Their integrated (in time) energy and their duration of energy release that carry a lot of information about the energy of flares over the entire range of energy in addition to the conventional characteristics of flares, characterizing their class in the X-ray band. X-ray observations of solar flares is more suitable for statistical analysis of their energetics. They have the advantage over the optical solar observations of flares, where it is necessary to integrate

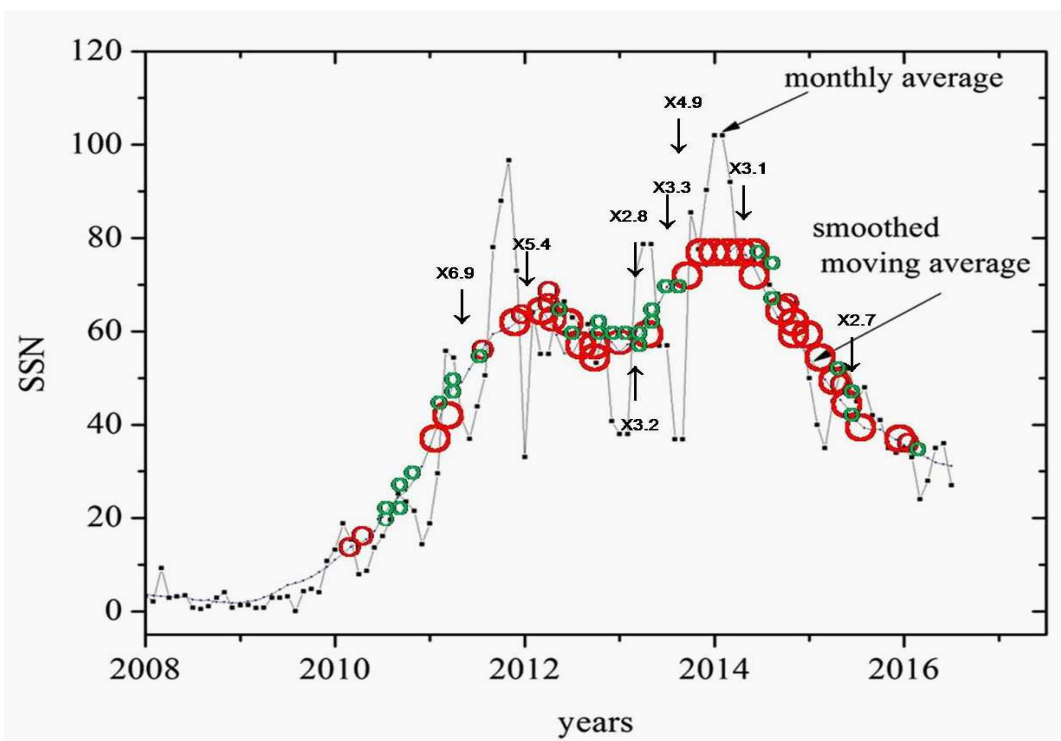


Figure 4: The distribution of the number of flares (monthly average) in cycle 24. The arrows point out to the strongest flares. Small circles shows the months when numbers of flares (M1 – X7 classes) for a month are less than 10. The large circles shows the months when numbers of flares are more than 10 flares per month.

over the surface of the flares.

In Figure 5 we can see that flare energy  $E$ , as the most important feature of a flare impact on the earth’s atmosphere, has not the close relationship with the amplitude of the flare in soft X-rays. We have calculated the values of the total energy  $E(J \cdot m^{-2})$  in the range 0.1 – 0.8 nm at the level of the earth’s atmosphere for 115 flares. Evaluation of energy of optical flares in [Hudson, 1991] showed that the distribution of their integral in time of the values of the energies can be represented by a power function  $N \sim E^{-\beta}$ . The universality of this distribution was proved for X-rays flares. The measure of the energy spectrum  $\beta$  was markedly changed in different phases of the 11-yr cycle. In [Sotnikova, 2010] the study of energy spectra of flares in the

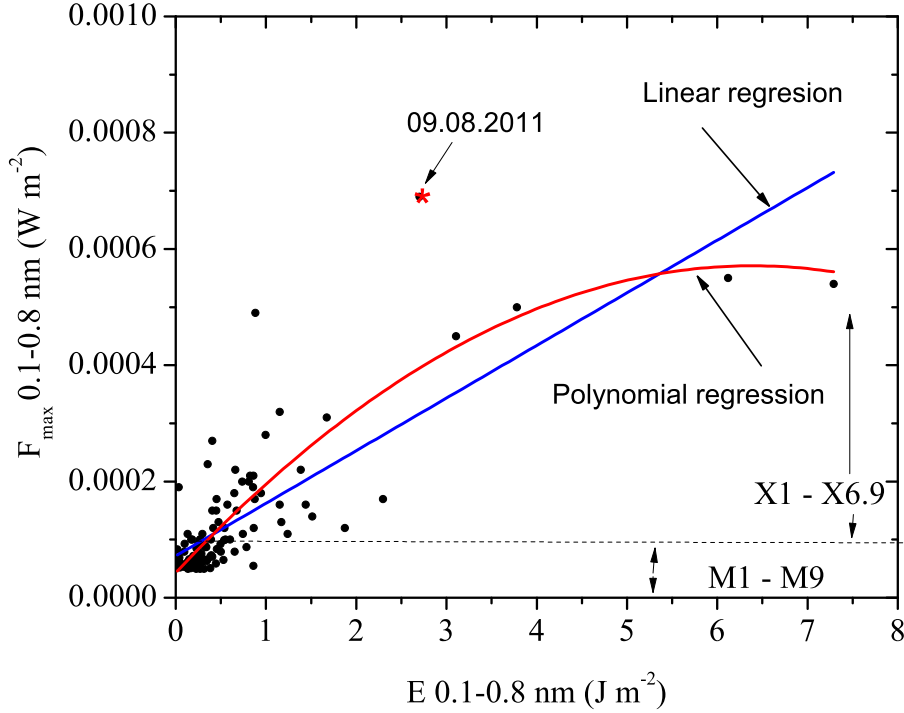


Figure 5: The dependence of the flare’s amplitude  $F_{max}$  versus the total energy of the flare  $E$  according GOES-15 0.1 – 0.8 nm observational data. The analysis is presented for the flares of M5 – X7 classes. The flare 09.08.2011 is pointed with the asteric.

soft X-rays band during solar cycles 21 and 22, for each year separately, was made. It was shown that the spectrum index  $\beta = d\log E/d\log N$  depends on the rise phase, the maximum and the minimum of the 11-yr cycle. It was also obtained that the yearly average energy of flares for each year of the cycle significantly vary with the phase of the cycle, increasing in overall from minimum to maximum of the cycle.

For 115 flares of M5 – X7 class of cycle 24 we have built the energy spectrum. The energy spectrum of the flares – is the number of flares with a certain total energy (in the soft X-ray interval 0.1 – 0.8 nm) versus the value of this total energy – has been constructed by us using data from the satellite

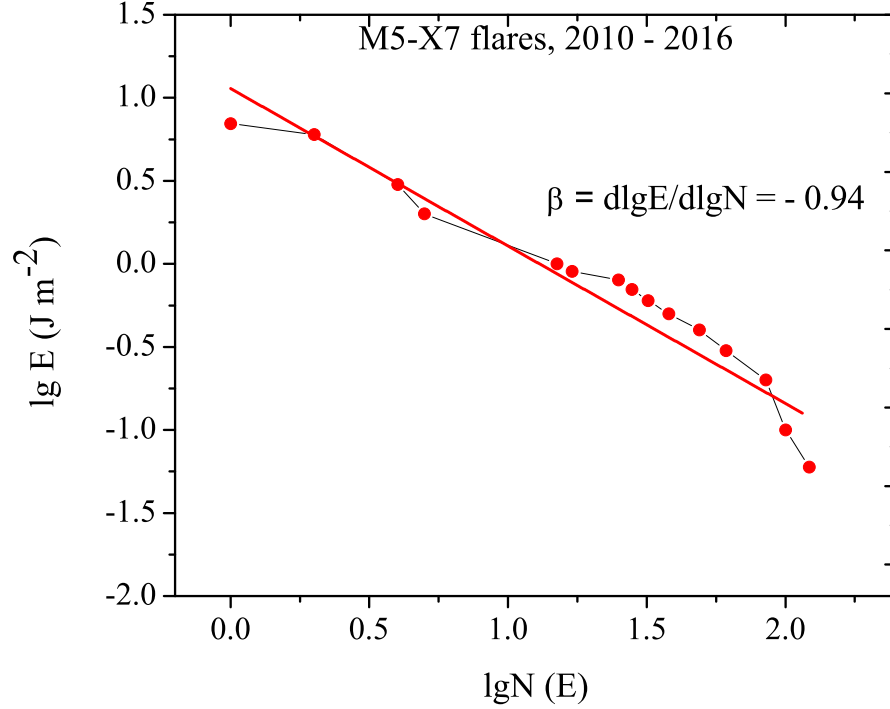


Figure 6: The energy spectrum of the flares is the number of flares with a certain total energy (in the soft X-ray interval 0.1 – 0.8 nm) versus the value of this total energy, constructed by us using data from the satellite GOES-15. The distribution of the number of flares with a certain energy depending on the energy values of the flares, we can imagine as the exponential function  $N \sim E^{-\beta}$ .

GOES-15. Figure 6 shows that the absolute value of  $\beta$  in cycle 24 corresponds to the phase of maximum of the 11-yr cycle according to [Sotnikova, 2010]. The straight line marks the dependence  $\beta = d \log E / d \log N = -0.94$ .

### 3 THE LARGEST FLARE OF X-RAY CLASS X6.9 IN CYCLE 24

Schrijver [2016] has studied large flares (M5 – X7 classes) based on SDO/AIA observations and showed that full-disk emission images of the corona and transition region, the Measure of Emission (ME) of lines, the dynamics of the surface magnetic fields differed in different flares and out of flares. The AIA (Atmospheric Imaging Assembly) was launched as a part of NASA Solar Dynamics Observatory (SDO) mission; irradiance products from AIA are available at AIA website, <https://sdo.gsfc.nasa.gov/data/aiahmi/>. AIA will advance our understanding of the mechanisms of solar variability and of how the energy of the Sun is stored and released into the heliosphere and geospace, [Lemen et al., 2012].

The EVE (Extreme ultraviolet Variability Experiment) instrument, and its calibration, are well understood [Woods et al., 2012]. A key aspect of the SDO satellite in geosynchronous orbit (GEO) is that it provides continuous solar observations with very few Earth eclipses. Irradiance products from EVE are available in a variety of wavelength resolutions and time cadences from the EVE website, [http://lasp.colorado.edu/eve/data\\_access/service/](http://lasp.colorado.edu/eve/data_access/service/)

For large flares, a significant amount of heating energy could be provided during the decay phase, sometimes more than during the rise phase observing the movement of X-ray emission source, put forward that the continuous heating into the decay phase is in the form of "sequential heating of new loops in the flare region" [Qiu and Longcope, 2016]. We have analyzed the flare of X-ray class X6.9 to compare the fluxes and the development of the flare in the range of wavelengths from the soft X-rays ( $\lambda = 0.1 - 0.8$  nm) until to the extreme ultraviolet ( $\lambda \leq 30.4$  nm), see Figure 7 and Table 1. The EUV solar irradiance is made by the EVE instrument aboard NASA's Solar Dynamics Observatory.

On the example of X6.9 flare (09.08.2011), we analyzed the sequence of the beginning of the impulsive phase of flare in different lines of the EUV-range. The excellent SDO observations with a resolution of 1 minute allow to determine the delay between the beginning of the flare in different lines.

Figure 7 shows that the level of the absolute values of fluxes in the studied lines of the EUV-range according to the SDO/EVE data varies from  $3 \cdot 10^{-5} (Watt \cdot m^{-2})$  at the line 33.5 nm to  $5 \cdot 10^{-4} (Watt \cdot m^{-2})$  from the strongest

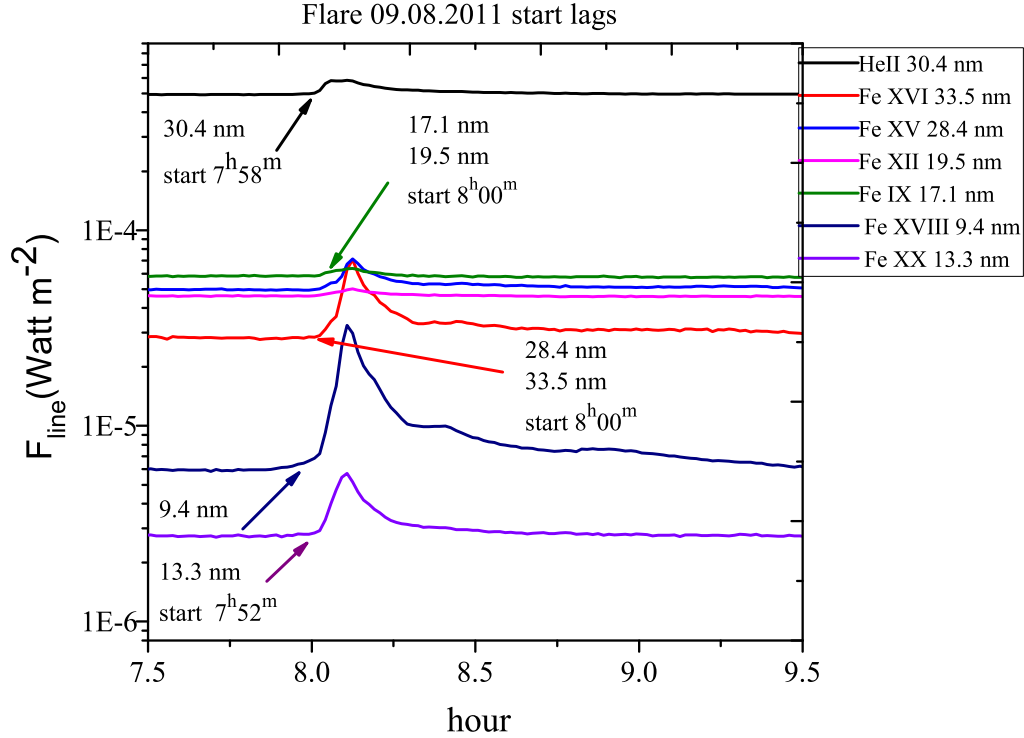


Figure 7: The development of the largest flare in cycle 24 of X6.9 class observed 9.08.2011 at different wave-lengths of EUV-range. Observations of SDO/EVE.

line of the EUV-range 30.4 nm. In Figure 7 we can see that the beginning of the studied flare X6.9 in different lines occurs at different times, and the time of maximum in these lines occurs almost simultaneously. For this flare according to TIMED (Thermosphere, Ionosphere, Mesosphere, Energetics and Dynamics) observations (<http://science.nasa.gov/missions/timed/>) the increase of the radiation flux was: in the range 0.1 – 7 nm – 44 000 times, in the line 30.4 nm (HeII)  $\sim 20\%$ ; in the line 121.6 nm (*Lyman* –  $\alpha$ )  $\sim 8\%$ .

Table 1 shows the summary of SDO/EVE observations in 8 EUV-lines and in the X-ray interval of 0.1 – 0.8 nm in which we can see the lags in different lines of flare beginning. We note that the moments of beginning of flare in different lines of the EUV-range (SDO/EVE) and in Soft X-ray 0.1

Table 1: The largest flare of cycle 24 – X6.9 according to the X-ray classification. The moments of flare beginning and flare maximum in different lines of the EUV-range according to SDO/EVE and in soft X-ray (SXR) 0.1–0.8 nm according to GOES-15.

Wavelength (nm)	Ion, Satellite	Flare begin. (UT)	Flare max. (UT)
9.4	FeXVIII, SDO	7:50-7:51	8:05-8:06
13.3	FeXX, SDO	7:52-7:53	8:06-8:07
0.1–0.8	SXR, GOES-15	7:54-7:55	8:05-8:06
13.1	FeVIII, SDO	7:56-7:57	8:06-8:07
30.4	HeII, SDO	7:58-7:59	8:05-8:06
33.5	FeXVI, SDO	8:00-8:01	8:06-8:07
28.4	FeXV, SDO	8:00-8:01	8:07-8:08
19.5	FeXII, SDO	8:00-8:01	8:06-8:07
17.1	FeIX, SDO	8:00-8:01	8:07-8:08

– 0.8 nm (GOES-15) lagged each other in different lines at 2 – 5 minutes.

We can see from the Table 1 that this X6.9 flare began, first in lines Fe XX (13.3 nm) and in line Fe XVIII (9.4 nm). These lines are formed in flaring corona at a temperature of  $\log(T) = 6.8 \div 7.0$ . Then the flare starts in the range of 0.1-0.8 nm. In the lines Fe XVI (33.5 nm), Fe XV (28.4 nm), Fe IX (17.1 nm) and in the line He II (30.4 nm) the flare starts later. These lines are formed in active-region corona and transition region at a temperature of  $\log(T) = 5.0 \div 6.0$ , see Table 2, Fig. 8.

Table 2 shows how the different ions which are involved in the formation of bright EUV-spectral lines are distributed with height in solar atmosphere. Figure 8 in accordance with Table 2 demonstrates the distribution with height of the regions of the EUV-lines formation according to the Atmospheric Imaging Assembly (AIA) provides multiple simultaneous high-resolution full-disk emission images of the corona and transition region, in the EUV-band lines: FeXVIII (9.4 nm), FeVIII, XXI (13.1 nm), FeIX (17.1 nm), FeXII, XXIV (19.3 nm), FeXIV (21.1 nm), HeII (30.4 nm), and FeXVI (33.5 nm).

Figure 7 shows that there are the shifts of the moment of the flare beginning in different spectral lines according SDO/EVE and GOES-15 observations of the flare X6.9 that occurred 09.08.2011. The same flare was studied in detail in [Sharykin, et al., 2015], where the Plasma Heating to Ultrahigh Temperatures was analyzed. A model of flaring region in the two-temperature

Table 2: The primary ions observed by SDO. Many are species of iron covering more than a decade in coronal temperatures.

Channel (nm)	Primary ion(s)	Region of atmosphere	log(T)
30.4	HeII	transition region, upper photospher	4.7
160.0	CIV + cont.	quiet corona, upper photospher	5.0
17.1	FeIX	quiet corona, transition region	5.8
19.3	FeXII, XXIV	corona and hot flare plasma	6.2, 7.3
33.5	FeXVI	active-region corona	6.4
9.4	FeXVIII	flaring corona	6.8
13.1	FeVII, FeXX	transition region,flaring corona	5.6, 7.0

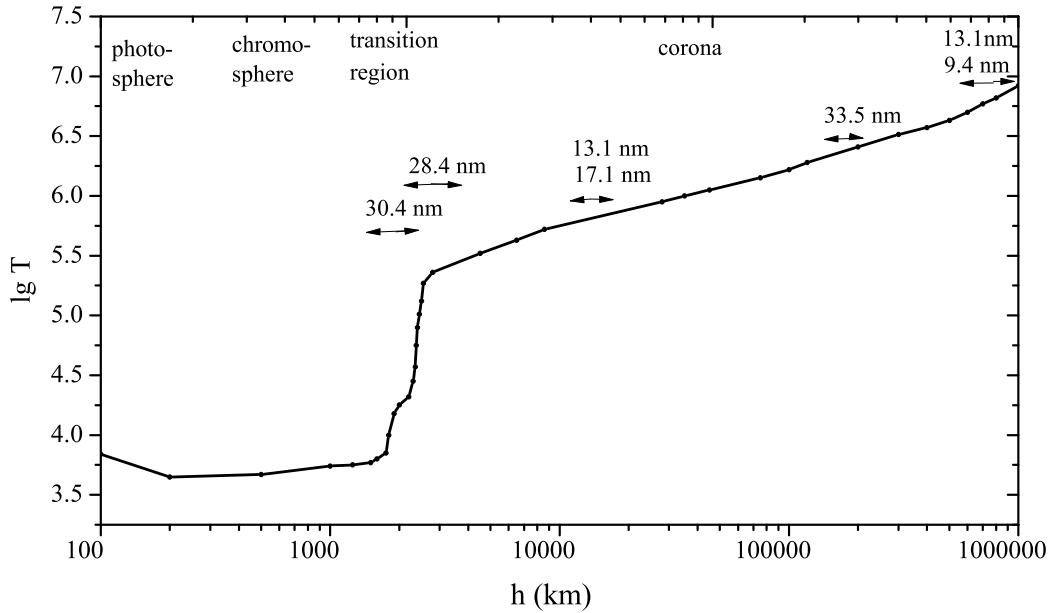


Figure 8: The temperature of solar atmosphere change of with height. The regions of the solar atmosphere corresponding to the maximums of fluxes in the lines HeII 30.4 nm, FeXV 28.4 nm, FeXXI 13.1 nm, FeIX 17.1 nm, FeXVI 33.5 nm and FeXVIII 9.4 nm are marked.

approximation is presented in [Sharykin, et al., 2015]. It was assumed that in the upper part of the flare loop exists the area with the super hot (sh) plasma. The observed plasma in the sh-region is assumed as a source of non-thermal electrons and is associated with their acceleration. The sh-region lies closest to the proposed site of the initial energy release in the corona (the region of magnetic reconnection). The population of nonthermal electrons is entered to lower levels till hot-region and further into the dense part of the solar atmosphere. This leads to evaporation of the chromosphere. The transfer processes occur along the force lines of the magnetic field, the heat transfer occurs inside the flare loop. The fluxes in coronal lines increase during the process of plasma heating in the flare due to the increase of the emission measure. This model corresponds to our study, according to which the fluxes increase, first in lines 9.4 nm and 13.1 nm and in the end when nonthermal electrons reach the chromospheric condensation, the fluxes increase in lines 28.4 nm and 30.4 nm. Table 1 shows that this flare first starts brightening in the lines formed in the corona at a temperature of  $\log(T) = 6.8 \div 7.0$  and then starts in the lines formed in the low corona and transition zone at a temperature of  $\log(T) = 5.0 \div 5.5$ .

## 4 CONCLUSIONS

The flare activity in cycle 24 was significantly lower than in cycles 21 – 23 according to the observational data (GOES-15, M1 – X7 class) and SDO/EVE (EUV – range). Our analyzing of the solar activity in cycle 24 and the study of the large flare of X6.9 class in the range of wavelengths from the soft X-ray until to the extreme ultraviolet showed the following:

- The peculiarity of the investigated flare activity is that the coefficient of linear correlation  $k$  for the dependences "FI versus other solar indices" calculated for the 2010 – 2016 is equal  $k \sim 0.65 \div 0.75$  in cycle 24, less than  $k$  in cycles 21 – 23 ( $k \sim 0.75 \div 0.85$ ), see [Bruevich et al., 2014].
- Most of large flares (X-ray class  $>X2.7$ ) occurred in the rise phase and in the maximum of cycle 24. Unlike the large flares in cycles 21, 22 and 23, where the greatest number of flares were observed during the decline phases.
- It is shown that for the analysis of the impact of solar flares on the atmosphere of the earth it is necessary to consider the total energy of flares

- E. Unlike the  $F_{max}$  – the maximum amplitude of the flare flux in the range of 0.1 – 0.8 nm, see Figure 5.
  - We have constructed the energy spectrum of flares in cycle 24 using the data from the satellite GOES-15 for the 115 flares of the X-ray class  $> M5$ . This index of the energy spectrum  $\beta$  for 115 flares in cycle 24 corresponds to the phase of maximum of the cycle.
  - The SDO/EVE and GOES-15 observations for the largest flare (X6.9) of cycle 24 that occurred 09.08.2011 showed that the shift of the moment of the flares beginning in the spectral lines 9.4 nm and 13.3 nm was for about 3 – 4 min relative to the moment of the flares beginning in 0.1 – 0.8 nm region, was about 5 – 6 minutes relative to the start time of the flare in the spectral line 30.4 nm and was about 7 – 8 min relative to the start time of the flare in the spectral lines of 17.1 nm, 19.5 nm, 28.4 nm and 33.5 nm, see Table 1.

## References

- [1] Atac, T. 1987, *Astrophysics and Space Science*, **135**, 201.
- [2] Avakyan S., Voronin N. 2012, *Academy of energy (In Russian)*, **5**, 24.
- [3] Bruevich E.A., Yakunina G.V. 2015, *Geomagnetism and Aeronomy*, **55**, N8, 1060.
- [4] Bruevich E.A., Bruevich V.V. and Yakunina G.V. 2014, *J. Astrophys. Astron.*, **35**, N1, 1.
- [5] Hudson H. 1991, *Solar Physics*, **133**, 357.
- [6] Qiu J., Longcope D. 2016, *ArXiv e-print.*, ArXiv:**1604.05342**.
- [7] Khlystov A.I. and Somov B.V. 2012, *Izvestiya, Atmospheric and Oceanic Physics*, **48**, N7, 717.
- [8] Khlystov A.I. 2014, *Izvestiya, Atmospheric and Oceanic Physics*, **50**, N8, 776.
- [9] Lemen, J.R., Title, A.M., Akin, D.J. et al. 2012, *Solar Physics*, **275**, 17.
- [10] Nagovitsyn Y., Pevtsov A., Livingston W. 2012, *Astrophysical Journal Letters*, **758**, L20.

- [11] Nusinov A., Kazachevskaya T. 2006, *Solar System Research*, **40**, 111.
- [12] Pevtsov A., Nagovitsyn Y., Tlatov A., Rybak A. 2011, *Astrophysical Journal Letters*, **742**, L36.
- [13] Pevtsov A., Bertello L., Tlatov A, Kilcik A., Nagovitsyn Y. 2014, *Solar Physics*, **289**, 593.
- [14] Schrijver C. 2016, *ArXiv e-print.*, ArXiv:**1602.07244**.
- [15] Sharykin I., Struminsky A., Zimovets I. 2015, *Astronomy Letters*, **41**, 53.
- [16] Sotnikova R.T. 2010, *Geomagnetism and Aeronomy*, **50**, N7, 905.
- [17] NOAA NGDC space weather, solar indices data. 2016, <http://www.ngdc.noaa.gov/stp/space-weather/solar-data/solar-indices>.
- [18] Woods, T.N., et al. 2012, *Solar Physics*, **275**, 115.